Solution and Solid Trinitrotoluene (TNT) Photochemistry: Persistence of TNT-like Ultraviolet (UV) Resonance Raman Bands

Katie L. Gares, Sergei V. Bykov, Bhaskar Godugu, Sanford A. Asher*

Department of Chemistry, University of Pittsburgh, Pittsburgh, PA 15260 USA

We examined the 229 nm deep-ultraviolet resonance Raman (DUVRR) spectra of solution and solid-state trinitrotoluene (TNT) and its solution and solid-state photochemistry. Although TNT photodegrades with a solution quantum yield of $\varphi \sim 0.015$, the initial photoproducts show DUVRR spectra extraordinarily similar to pure TNT, due to the similar photoproduct enhancement of the $-NO_2$ stretching vibrations. This results in TNT-like DUVRR spectra even after complete TNT photolysis. These ultraviolet resonance Raman spectral bands enable DUVRR of trace as well as DUVRR standoff TNT detection. We determined the structure of various initial TNT photoproducts by using liquid chromatography-mass spectrometry and tandem mass spectrometry. Similar TNT DUVRR spectra and photoproducts are observed in the solution and solid states.

Index Headings: **Ultraviolet resonance Raman spectroscopy; UVRRS; Trinitrotoluene photochemistry; TNT photochemistry; Liquid chromatography mass spectrometry; LCMS; Standoff detection; Explosives; Energetic materials.**

INTRODUCTION

There is intense interest in the standoff detection of trace quantities of explosives on surfaces because of the increasing threats posed by improvised explosive devices (IEDs).[1–5] The methods presently being investigated for standoff detection mainly involve spectroscopy, where a light source probes a distant surface and the spectral response is monitored in order to detect explosive molecular species. Standoff detection obviously improves safety for the spectroscopists.[4,5] This intense interest in developing standoff detection methods, unfortunately, is severely challenged by the difficulty of devising methods with sufficient sensitivity.[1,4]

Raman spectroscopy is one of the few spectroscopic methods that can be developed for standoff detection of dilute analytes. Numerous investigations have probed the utility of normal Raman spectroscopy for explosive detection.[1–10] These normal Raman spectral studies, with excitation in the visible spectral region, while promising, have not demonstrated sufficient signal to noise (S/N) to be clearly applicable for standoff detection.

More recently deep-ultraviolet resonance Raman (DUVRR) spectroscopy has been investigated as a standoff detection method.[1,4,11] It has the potential for increased sensitivity to explosive molecules because of resonance enhancement and the increased Raman cross sections that result from the increased excitation frequencies. In addition, increased DUVRR spectra signal-to-noise ratios occur because there is an absence of competing relaxed fluorescence in condensed phase samples, due to the lack of significant fluorescence at $\lambda < 260$ nm.[1,11,12] Most explosives have their first allowed electronic transitions in the UV region below 250 nm.[11]

The prognosis for DUVRR standoff detection is still unknown because the overall sensitivity depends on unknown phenomena, such as the attenuation from self-absorption and the potential interferences that derive from analyte photochemistry as well as the photochemistry of interfering background species. This photochemical interference could result from phenomena such as the loss of analyte spectral intensities due to photodestruction of the analyte, or from interfering spectral contributions from new photoproduct species that derive from the analyte or from other species.[13] Furthermore, it is well known that some explosives thermally degrade and that some explosives such as trinitrotoluene (TNT) can be photolyzed by near UV irradiation from the sun.[14] In order to determine whether DUVRR will work for standoff explosive detection, it is necessary to characterize the DUVRR of the explosive molecules as well as their photodegradation products.

In this paper, we examine the photochemistry of solid and solution TNT by using 229 nm DUVRR. The maximum of the TNT's main absorption band occurs at 229 nm.[11] This excitation wavelength gives rise to a maximal resonance enhancement of the TNT Raman bands, maximizing the TNT Raman cross sections.[11] This strongly absorbed wavelength initiates facile TNT photochemistry.[14–18] We also characterize some of the initial TNT photoproducts.

EXPERIMENTAL

Raman Measurements. The ultraviolet Raman (UVR) spectrometer was described previously.[19,20] The ultraviolet resonance Raman (UVRR) spectra were excited by continuous wave (CW) 229 nm light generated by using a Coherent Industries Innova 300 FreD frequency doubled Ar^+ laser.[19] A Spex Triplemate spectrograph and a Princeton Instruments charge-coupled device (CCD) camera (Spec-10 System, Model 735-0001) were used to disperse and detect the Raman scattered light.

Solution Samples. Deep-ultraviolet resonance Raman measurements of 1.0 mg/mL TNT solutions in CH_3CN (EMD Chemicals) or CD_3CN (Acros Organics)

Received 27 June 2013; accepted 9 September 2013.

* Author to whom correspondence should be sent. E-mail: asher@pitt.edu.

DOI: 10.1366/13-07190

0003-7028/14/6801-0049/0

utilized accumulation times of 5 min per spectrum measured. Deep ultraviolet resonance Raman of CD_3CN, CH_3CN, and the quartz cell were separately measured.

Different conditions were used for the photodegradation experiments. The exposure was normalized to absorbed photons/molecule to compare the data between experiments. In the DUVRR photodegradation experiment, a 1.5 mL solution of 1 mg/mL concentration of TNT in CD_3CN (Acros Organics) was placed in a 1 cm path length, fused-silica, temperature-controlled cuvette kept at 20.0 °C. The solution was continuously stirred with a magnetic stir bar and excited over a total of 9.5 h by a focused (~80 μm diameter) 10 mW 229 nm CW laser beam. An initial spectrum was measured during the first 5 min, and then spectra were measured after 30, 90, 150, 210, 270, 330, 390, 450, 510, and 570 min (5, 16, 26, 36, 47, 57, 67, 78, 88, and 98 photons/molecule). Another photodegradation experiment was performed for the liquid chromatography–mass spectrometry and tandem mass spectrometry (LC–MS/MS) measurements using 1.5 mL of 0.25 mg/mL TNT in CH_3CN solution in a 1 cm path length fused-silica cuvette. It was irradiated for a total of 4 h and 45 min by 5 mW of a 229 nm CW laser beam. Here, 100 μL aliquots were taken at 15, 105, 225, and 285 min (5, 36, 78, and 98 photons/molecule) for LC–MS/MS measurements.

In order to investigate the DUVRR spectra of potential photoproducts of TNT, we purchased the potential photoproducts that were commercially available. Generally, the photoproducts are unstable and unsafe when dried in the solid state, so we kept the compounds in the original solvent they were purchased in for the DUVRR, ultraviolet visible (UV/Vis), and LC–MS experiments. The standards of 2-amino-4,6-dinitrotoluene (DNT), 4-amino-2,6-DNT, and 3,5-dinitroaniline came dissolved in CH_3CN. The 2,5-dinitrophenol (DNP) was received as a wet powder. We dissolved it in both water and CD_3CN. The solvent CD_3CN was used in the photodegradation experiments since CD_3CN has no overlapping Raman bands in the 1100–2000 cm^{-1} TNT spectral region. Deep-ultraviolet resonance Raman with 229 nm light was used to measure 0.5 mL samples of 1 mg/mL 2-amino-4,6-dinitrotoluene (Supleco Analytical), 4-amino-2,6-dinitrotoluene (Supleco Analytical), and 3,5-dinitroaniline (Thermo Scientific Acros Organics) in CH_3CN with spectral accumulation times of 3 min. Deep-ultraviolet resonance Raman using 229 nm light was measured of 1 mg/mL 2,5-dinitrophenol (2,5-DNP; Aldrich) in CD_3CN with a spectral accumulation time of 5 min.

Solid Samples. A total of 350 mg of MgF_2 (Strem Chemicals) was ground to a fine powder. A volume of 0.2 mL of a 1 mg/mL TNT solution in CH_3CN was added and the system left to evaporate. The dried sample was ground and packed into the groove of a brass rotating Raman cell that was spun during excitation. Raman spectra were measured by using 10 mW of 229 nm CW laser excitation with a laser spot size diameter of ~80 μm at the sample surface. Laser excitation occurred in an almost backscattering geometry (150°) over a 3 min period over which 18 spectra were measured with integration times of 10 s each. A Teflon Raman spectrum was measured for Raman frequency calibration. The Raman spectra of solid 2-amino-4,6-dinitrotoluene (DNT), 4-amino-2,6-DNT, and 3,5-dinitroaniline (3,5-DNA) were also measured as described above using the 1 mg/mL solutions of the derivatives. Na_2SO_4 was added to the solid samples as an internal standard to estimate the Raman cross sections.

Absorption Measurements. A 1.5 mL sample of 1 mg/mL TNT in CH_3CN was irradiated with ~10 mW of 229 nm CW light focused to an 80 μm spot diameter for 9.5 h. During this irradiation, 75 μL aliquots were taken after 0, 30, 210, 450, and 570 min of irradiation. Absorption spectra were measured by using a 0.05 mm path length fused-silica cuvette and a Varian Cary 5000 UV-Vis/near-infrared (NIR) spectrometer. Absorbance spectra were also measured of 1 mg/mL 2-amino-4,6-DNT, 4-amino-2,6-DNT, 3,5-DNA, and 2,5-DNP in CH_3CN using the 0.05 mm path length fused-silica cuvette.

Liquid Chromatography–Mass Spectrometry Measurements. In order to obtain information on the photochemical products, LC–MS/MSs were measured of 0.1 mL aliquots obtained after specific illumination times. The samples were measured using the Dionex-UltiMate 3000 Rapid Separation LC System and the Thermo Scientific Q-Exactive high-resolution mass spectrometer (HRMS). Electrospray ionization (ESI) in the negative ionization mode was used to analyze the samples. A 150 mm × 2 mm diameter Jupiter column containing 3 μm diameter C-18 silica particles was used along with an isocratic elution method consisting of a mobile phase of 50/50 methanol/water. The flow rate was 0.2 mL/min with a total run time of 20 min. Liquid chromatography–mass spectrometry and tandem mass spectrometry was also measured of 0.1 mL samples of 1 mg/mL 2-amino-4,6-DNT, 4-amino-2,6-DNT, and 3,5-DNA in CH_3CN and 2,5-DNP in water.

Liquid chromatography–mass spectrometry was also measured for the solid TNT photochemical products at various illumination times. The surface of two ~45 mg samples of the fine powder containing TNT, MgF_2, and Na_2SO_4 were irradiated for 10 and 20 min. Once irradiated, the samples were extracted with CH_3CN and centrifuged. The extract was monitored by LC–MS. The analysis method utilized a combination of ESI and atmosphere pressure chemical ionization (APCI) using the negative ionization mode with the Shimadzu LCMS2020. The mobile phase consisted of CH_3CN and 0.1% formic acid. The gradient elution began using 10% of CH_3CN and gradually increased to 90% CH_3CN over a 13 min period. The gradient remained constant until 16 min, whereupon the elution decreased to 10% CH_3CN at 20 min. The flow rate was 0.2 mL/min with a total run time of 20 min.

RESULTS

Figure 1A shows that the DUVRR intensities of TNT dissolved in CD_3CN decays rather slowly with time. The strongest band at 1357 cm^{-1} derives from a TNT vibration where $-NO_2$ symmetric stretching is coupled to C–N stretching. The 1549 and 1622 cm^{-1} peaks derive from vibrations where aromatic ring stretching couples to $-NO_2$ asymmetric stretching.[11,21,22] The 1210 cm^{-1} band derives from a vibration that primarily involves symmetric aromatic ring breathing motion.[11,21–23] The band at

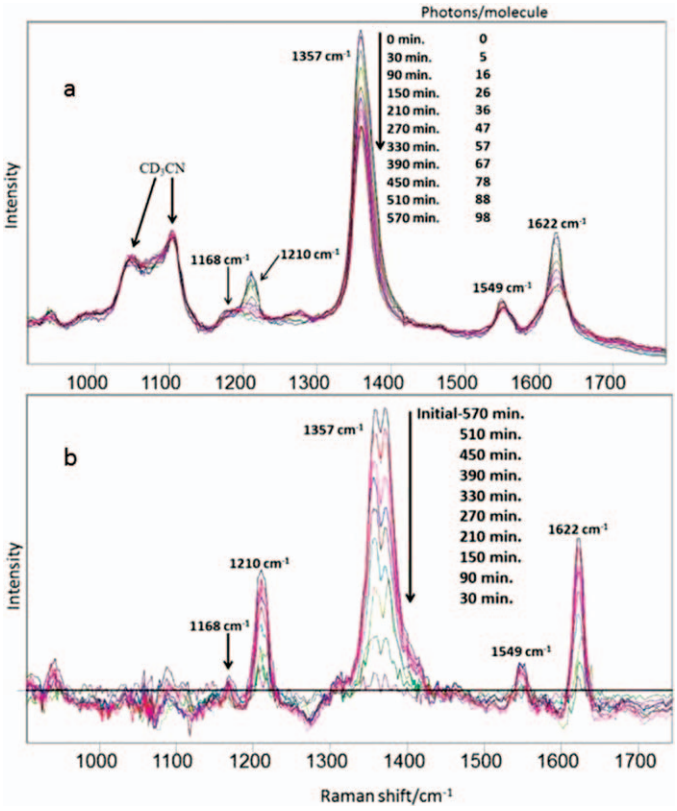

FIG. 1. (**a**) Irradiance time dependence of DUVRR spectra. Here, 1.5 mL of 1 mg/mL TNT in CD_3CN was irradiated with 10 mW of 229 nm UV light. The TNT spectra were normalized to the CD_3CN 2117 cm^{-1} band intensity and the silica bands subtracted. The CD_3CN was not subtracted. The absorbed photons/molecule is shown. (**b**) TNT difference spectra (initial spectrum minus spectra irradiated for t = 30, 90, 150, 210, 270, 330, 390, 450, 510, and 570 min). Negative features result from photoproduct Raman bands.

1168 cm^{-1} derives from C–C ring in-plane trigonal bending that also contains C–N and C–CH_3 stretching.[11,21,22]

The 1210 cm^{-1} TNT Raman band completely disappears over the 450 min irradiation time, indicating the complete photolysis of TNT. The 1210 cm^{-1} TNT marker band results from a dominantly aromatic ring vibration that occurs only for the specific ring substitution of TNT. As shown below, this band does not exist in the putative photoproduct spectra. The other TNT Raman bands show much smaller relative intensity decreases as well as band shape changes.

The lack of disappearance of these other bands results from the overlapping contributions of photoproduct Raman bands at frequencies similar to the dominant bands of TNT; the vibrations involve similar $-NO_2$ stretching motions. These photoproduct Raman bands limit the intensity decrease of the 1357, 1549, and the 1622 cm^{-1} band intensities (by ~30% over the 570 min of irradiation). Even after the 1210 cm^{-1} TNT marker band disappears, the intense spectral features of the $-NO_2$ stretching vibrations from the photoproducts remain dominant. These strong spectral features allow UV Raman detection of TNT after long irradiation times subsequent to all TNT being photolyzed.

Figure 1B shows the difference spectra between the initial TNT spectrum and the later irradiation time

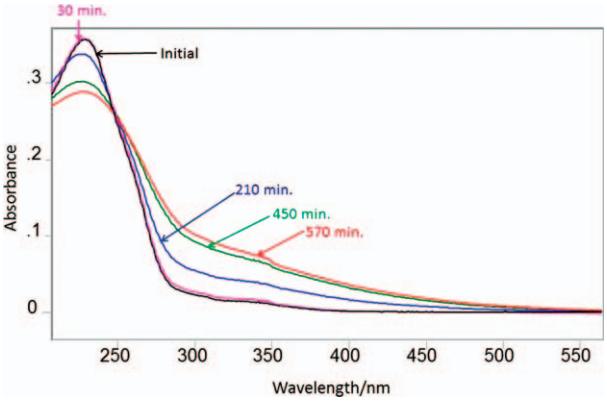

FIG. 2. Time dependence of the absorption spectra of TNT in CH_3CN after 0, 30, 210, 450, and 570 min irradiation by 229 nm light measured in a 0.05 mm path length cuvette.

DUVRR spectra of the TNT solutions. The troughs seen in the Fig. 1B difference spectra derive from photochemical product(s) bands.

Figure 2 shows the dependence of the absorption spectrum of TNT in CH_3CN on the irradiation time. After 30 min irradiation, the maximum absorbance at ~230 nm slightly increases and then monotonically decreases with time, while a broad shoulder appears between ~275–450 nm. The absorption spectra show complex changes as the TNT is photolyzed, presumably due to formation of numerous overlapping photoproduct absorption bands.

Previous studies of the photolysis of TNT showed multiple product formation pathways.[14,17] Trinitrotoluene shows significant absorbance in the near UV that can be excited by sunlight to give rise to photoproducts that may be similar to those formed with 229 nm excitation. With sunlight, photochemical reactions occur that lead to amine, hydroxyl, or carboxylic acid groups on the aromatic ring, while the aromatic ring stays intact.[17] Trinitrotoluene photolysis by sunlight forms initial photoproducts such as 4-amino-2,6-DNT or 2-amino-2,6-DNT, and 3,5-dinitroanline.[14] Another photoproduct formed in solutions of TNT in water undergoing ultraviolet radiation is 2,5-DNP.[24]

Figure 3 compares the solution DUVRR spectra of TNT to some of its possible photoproducts. The $-NO_2$ symmetric stretching Raman band at ~1357 cm^{-1} and the $-NO_2$ antisymmetric stretching Raman band at 1622 cm^{-1} are the strongest DUVRR features of TNT and are strongest in the mixture of photoproducts formed (especially evident in the solid state vide infra). Figure 3 shows that these photoproducts also display individual strong signature bands for each compound that involves specific aromatic ring vibrations. These occur at 1196 cm^{-1} for 2-amino-4,6-DNT, 987 cm^{-1} for 4-amino-2,6-DNT, 976 cm^{-1} for 3,5-dinitroaniline, and 1149 cm^{-1} for 2,5-DNP. These bands can be utilized to identify each photoproduct as it forms.

Figure 4 compares the TNT absorption spectrum to that of its putative photoproducts. Trinitrotoluene in CH_3CN shows an absorption maximum at ~229 nm that derives from the S_9/S_{10} electronic transitions[23] and a shoulder at ~260 nm that derives from its S_8 electronic transition.[23] A weaker absorption tail is evident in the

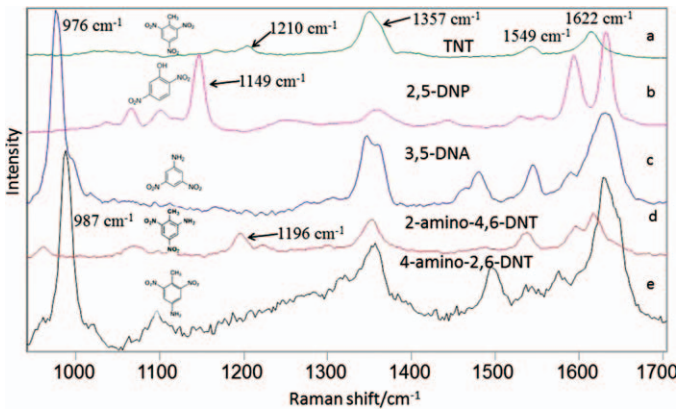

FIG. 3. 229 nm solution DUVRR spectra of 1 mg/mL TNT and possible photoproducts (in CH_3CN): (***a***) TNT, (***b***) 2,5-dinitrophenol (2,5-DNP; in CD_3CN), (***c***) 3,5-dinitroaniline, (***d***) 2-amino-4,6-dinitrotoluene, and (***e***) 4-amino-2,6-dinitrotoluene. The silica, CH_3CN, and CD_3CN contributions were subtracted. Spectra are scaled proportional to the Raman cross section (corrected for self-absorption and instrument function) of the most intense band in each spectrum: 1357 cm^{-1} band for TNT, 1149 cm^{-1} band for 2,5-DNP, 976 cm^{-1} band for 3,5-DNA, 1352 cm^{-1} band for 2-amino-4,6-DNT, and the 987 cm^{-1} band for 4-amino-2,6-DNT.

near UV that can absorb sunlight. Our recent TNT electronic state studies indicate that the C_s TNT conformer S_8 and S_9/S_{10} electronic transitions induce large changes in the $-NO_2$ group and aromatic ring electron densities.[23] The three putative photoproducts show higher 229 nm molar absorptivities than TNT does. These photoproducts also show larger features at longer wavelengths (~370–380 nm). A maximum absorbance at ~226 nm with a shoulder at ~270 nm and a feature at ~380 nm is seen for 2-amino-4,6-DNT. A maximum absorbance at ~230 nm with a second band at ~370 nm is seen for 4-amino-2,6-DNT. A maximum absorbance at ~226 nm with a shoulder at ~255 nm with a second band at ~390 nm is seen for 3,5-dinitroaniline. Three absorption bands at ~218 nm, ~272 nm, and ~360 nm are present for 2,5-DNP. The larger molar absorptivity of the photoproducts at 229 nm explain the initial increased absorption at 229 nm. The later decrease in the 229 nm absorption must result from the conversion of these photoproducts to other species.

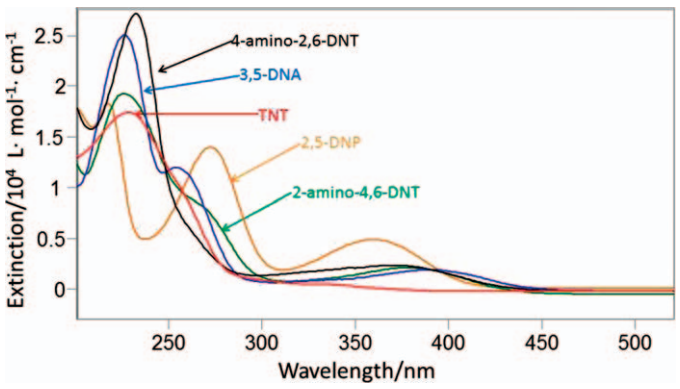

FIG. 4. Absorption spectra of 1 mg/mL TNT and its putative photoproducts: 2-amino-4,6-DNT, 4-amino-2,6-DNT, 2,5-dinitrophenol (2,5-DNP), and 3,5-dinitroaniline in CH_3CN measured in a 0.05 mm path length cuvette.

TABLE I. Absolute differential resonance Raman cross sections at 229 nm of TNT, 2-amino-4,6-DNT, 4-amino-2,6-DNT, 3,5-dinitroaniline, and 2,5-dinitrophenol in CH_3CN solution.

	Frequencies (cm^{-1})	229 nm resonance Raman cross sections (10^{-26} cm^2/molc·sr)
TNT	1168	2.8
	1210	3.8
	1357	15.7
	1549	3.3
	1622	9.2
2-amino-4,6-DNT	1196	6.1
	1351	9.8
	1537	4.6
	1593	3.2
	1618	10
4-amino-2,6-DNT	987	37.2
	1354	16.5
	1497	9.3
	1576	12.6
	1634	28.1
3,5-dinitroaniline	976	39.8
	1347	7.4
	1481	3.9
	1546	5
	1593	3.7
	1632	14.9
2,5-dinitrophenol	1069	3.5
	1149	11.7
	1272	3.2
	1358	1.6
	1595	7.9
	1633	9.3

The absolute differential resonance Raman cross sections that were measured for the DUVRR bands of TNT, 4-amino-2,6-DNT, 2-amino-4,6-DNT, 2,5-DNP, and 3,5-dinitroaniline are displayed in Table I. These resonance Raman (RR) cross sections were determined using the known cross section of the 919 cm^{-1} band of CH_3CN and corrected for self-absorption and the instrument function using the method described in Refs. 1 and 25.

Figure 5 shows the dependence of the TNT Raman band intensities upon the irradiation time and the number of photons absorbed. For this analysis, we fit each of the TNT DUVRR bands (Fig. 1A) to single Lorentzians except for the 1357 cm^{-1} $-NO_2$ symmetric stretching band that we fit to two overlapping Lorentzians. We determined the integrated intensities of these bands at each irradiation time. During irradiation, all the incident 229 nm light was absorbed by our optically thick TNT sample. Thus, we can calculate the average number of photons absorbed per TNT molecule at the different irradiation times; the total number of photons absorbed is identical to the number of incident photons.

We determined the photochemical quantum yield for the TNT photolysis in solution by measuring the 1210 cm^{-1} TNT signature Raman band (Fig. 5) time dependence.

The initial time-dependent rate of change of the TNT concentration is:

$$\frac{d[\mathrm{TNT}]}{dt} = -\varphi I / \mathrm{N_a} V \qquad (1)$$

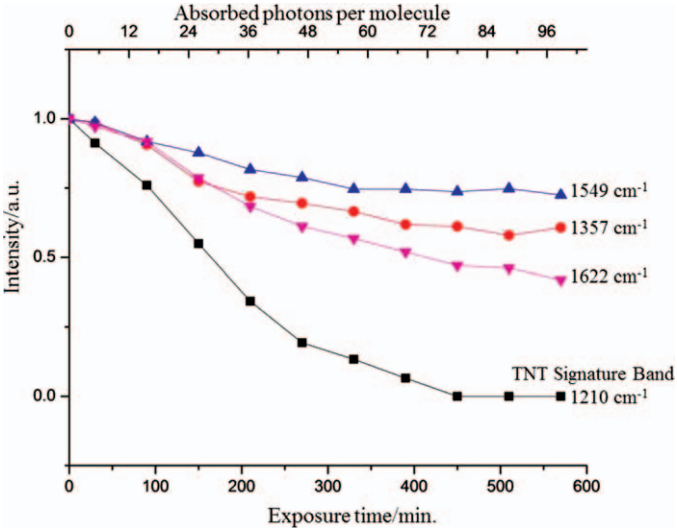

FIG. 5. Solution TNT Raman band intensities versus irradiation time or absorbed photons per molecule.

where [TNT] is the TNT concentration, φ is the quantum yield, *I* is the number of photons absorbed per TNT molecule per second, N_a is Avogadro's number, and *V* is the sample volume.

For our calculation, we fit the initial linear portion of the 1210 cm^{-1} band's exponential decay; its slope indicates a quantum yield of $\varphi = 0.015$ ($R^2 = 0.9986$).

In order to determine the photoproducts formed, we measured the LC–MS of the irradiated samples as shown in Fig. 6.

The chromatogram of the non-irradiated solution shows a single peak at ~6.30 min that derives from TNT. In contrast, the 15 min irradiated sample chromatograph shows the TNT peak and multiple peaks at different elution times resulting from photoproducts. As the irradiation time increases, the relative intensities of

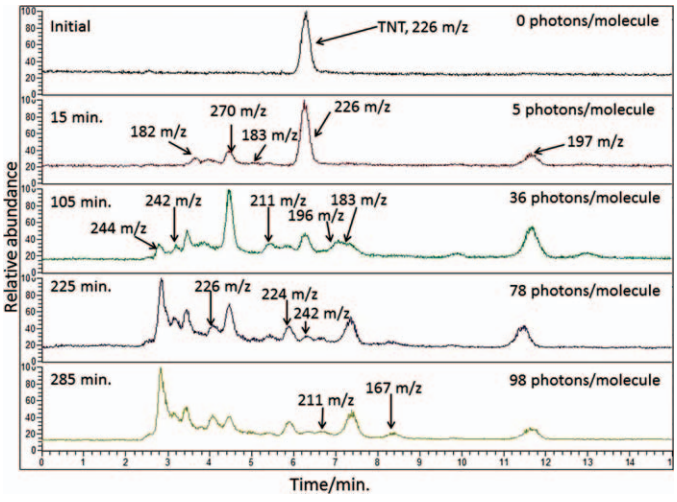

FIG. 6. Mass spectral ion current chromatograms of TNT irradiated with 229 nm light after different irradiation time intervals. After the 15 min spectrum, only newly eluted peaks are labeled in the 105, 225, and 285 min spectra that are not seen in the 15 min. Table II shows the m/z for every peak in each spectrum. The number of photons per molecule at each irradiation time is listed.

TABLE II. Mass chromatogram retention times, m/z values, and identity of species formed.

TNT sample	Retention time (min.)	m/z Peak	Species
Initial	6.3	226	TNT
15 min	3.5	182	3,5-DNA
	4.4	271	
	5.1	183	2,5-DNP
	6.3	226	TNT
	7.1	196	2-amino-4,6-DNT
	7.4	183	
	11.7	197	
105 min	2.4	244	
	3.2	242	
	3.5	182	3,5-DNA
	4.1	226	
	4.4	271	
	5.1	183	2,5-DNP
	5.2	211	
	6.3	226	TNT
	7.1	196	2-amino-4,6-DNT
	7.4	183	
	11.7	197	
225 min	2.4	244	
	3.2	242	
	3.5	182	3,5-DNA
	4.1	226	
	4.4	271	
	5.1	183	2,5-DNP
	5.2	211	
	5.9	224	
	6.2	242	
	6.6	211	
	7.1	196	2-amino-4,6-DNT
	7.4	183	
	11.7	197	
285 min	2.4	244	
	3.2	242	
	3.5	182	3,5-DNA
	4.1	226	
	4.4	271	
	5.1	183	2,5-DNP
	5.2	211	
	5.9	224	
	6.2	242	
	6.6	211	
	7.1	196	2-amino-4,6-DNT
	7.4	183	
	8.4	167	
	11.7	197	

the TNT peak decrease, while new peaks appear that derive from additional photoproducts. The mass chromatograms in Fig. 6 show the complexity of photoproducts formed.

The LC-MS data (Table II) indicates that multiple initial photoproducts are formed during the TNT photolysis. These have mass-to-charge ratios of 196, 197, 182, and 183 m/z. The 196 and 183 m/z peaks are small in the 15 min spectrum. At later times, additional photoproducts are formed. The 196 m/z photoproduct likely derives from an amino-dinitrotoluene derivative that is also reported in the recent sunlight-irradiated TNT photolysis studies that demonstrated 2-amino-4,6-dinitrotoluene or 4-amino-2,6-dinitrotoluene as TNT photoproducts with 196 m/z.[14,17] The 182 m/z photoproduct is likely 3,5-dinitrotoluene, which is also reported to be a sunlight-excited photoproduct of TNT.[14,17] The 183 m/z photoproduct is likely 2,5-dinitrophenol. The 197 m/z

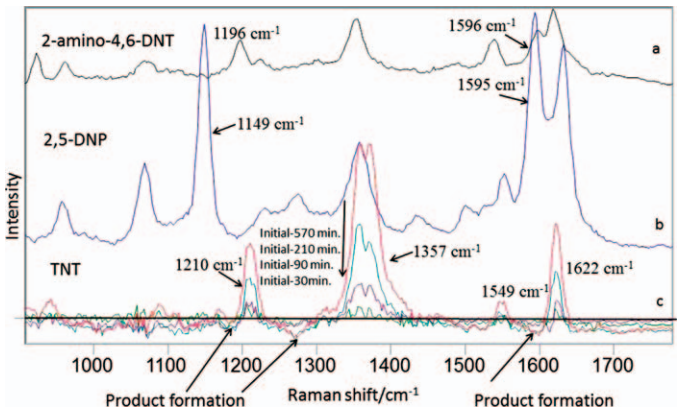

FIG. 7. 229 nm solution DUVRR spectra of 1 mg/mL (***a***) 2-amino-4,6-DNT (in CH_3CN), and (***b***) 2,5-dinitrophenol (in water), and (***c***) difference spectra of TNT (in CD_3CN) at times initial minus 30, 90, 210, and 570 min. The quartz, CH_3CN, and CD_3CN contributions have been subtracted. Negative features in spectrum (***c***) result from photoproduct contributions. Photoproduct contributions give rise to features at ~1196, ~1273, and ~1595 cm^{-1}.

photoproduct's molecular formula is $C_7H_6O_5N_2$, as given by the HRMS data. We could not obtain this compound to use DUVRR to determine its spectrum. It most likely results from a dinitrobenzyl alcohol as observed in the sunlight photochemical study.[14] The 183 m/z product at 7.1 min retention time has a molecular formula of $C_6H_4O_5N_2$, as given by the HRMS data. We were not able to determine its structure.

The HRMS data directly determines which 196 m/z DNT isomer forms in the initial stages of TNT photolysis (Fig. 6). The 4-amino-2,6-DNT derivative's MS/MS contains a peak at 149 m/z that makes it distinctly different from the 2-amino-4,6-DNT derivative's MS/MS spectrum. This 149 m/z peak is not present in the MS/MS of the 196 m/z peak of the TNT irradiated sample. Therefore, it is 2-amino-4,6-DNT that forms in the initial stages of photolysis. The MS/MS data also allowed us to determine some of the other initial photoproducts formed. We find that 3,5-DNA is the 182 m/z compound, and 2,5-dinitrophenol is the 183 m/z compound at the 5.1 min retention time. The pure MS/MS of 2,5-dinitrophenol matches the 183 m/z MS/MS from the irradiated samples, and the pure 3,5-dinitroaniline MS/MS matches the 182 m/z compound's MS/MS. The Supporting Information section contains the MS/MS data.

Figure 7 compares the 229 nm DUVRR solution spectra of 2-amino-4,6-DNT and 2,5-DNP to the TNT difference spectra at different irradiation times.

Above, 2-amino-4,6-DNT was determined to be one of the initial photoproducts formed (Fig.6). In Fig. 7C, a weak negative feature is seen at ~1196 cm^{-1} that likely corresponds to one of the lower intensity signature Raman bands of 2-amino-4,6-DNT, indicating that it is detectable as an initial photoproduct. Figure 7C also shows weak negative features at ~1273 and ~1596 cm^{-1} that likely correspond to two of the higher-intensity Raman bands of 2,5-DNP (Fig. 7B), indicating that it is detectable as another initial photoproduct.

Multiple initial photoproducts are formed (Fig. 6), indicating that TNT photolysis is complex even in the early stages of photolysis. With further photolysis, a

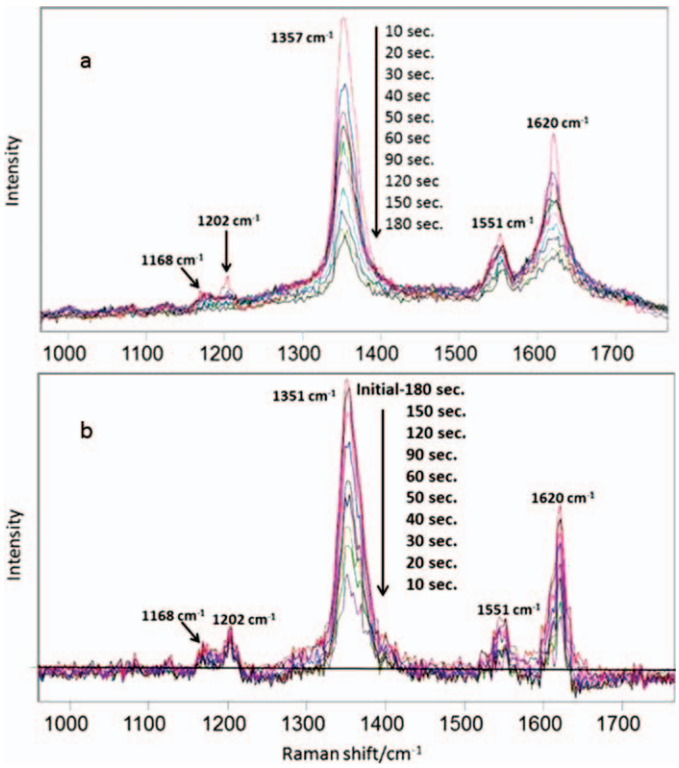

FIG. 8. (**a**) 229 nm excited, irradiation time dependence of the DUVRR of solid-state TNT on MgF_2 powder (0.06% mass fraction TNT). (**b**) Solid-state TNT difference spectra between initial spectrum and spectra measured at 10, 20, 30, 40, 50, 60, 90, 120, 150, and 180 s. Negative features derive from photoproduct band contributions.

complex mixture of photoproducts occur, many of which give rise to the overlapping Raman bands of the $–NO_2$ group attached to an aromatic ring. These remaining photoproduct bands give rise to persistent DUVRR TNT-like spectra that enable identification of trace TNT in DUVRR standoff detection studies.

Solid Trinitrotoluene Photolysis. We compared the photochemistry of solid-state TNT (Fig. 8A) to that of TNT in CD_3CN (Fig. 1A). The 1210 cm^{-1} TNT solution signature band occurs in the solid state at 1202 cm^{-1}. As in solution, this band quickly disappears upon irradiation (Fig. 8A).

As in TNT solutions, the strongest solid-state TNT DUVRR bands (Fig. 8A) involve $–NO_2$ stretching vibrations. The solid state TNT photoproducts also have their dominant Raman bands at frequencies similar to that of pristine TNT due to their similar $–NO_2$ stretching vibration resonance enhancement. The $–NO_2$ stretching vibration intensities decrease only slowly with irradiation time due to the photoproduct Raman intensity contributions. These strong photoproduct Raman bands give rise to TNT-like DUVRR spectra even after long irradiation times even after all of the TNT is photolyzed.

The DUVRR difference spectra between the initial and irradiated solid-state TNT (Fig. 8B) show photolysis of TNT and photoproduct formation similar to that in the solution. As seen in solution, there is a broad mixture of photoproducts forming.

Figure 9 shows the solid-state DUVRR spectra of TNT and its putative photoproducts. As in the solution

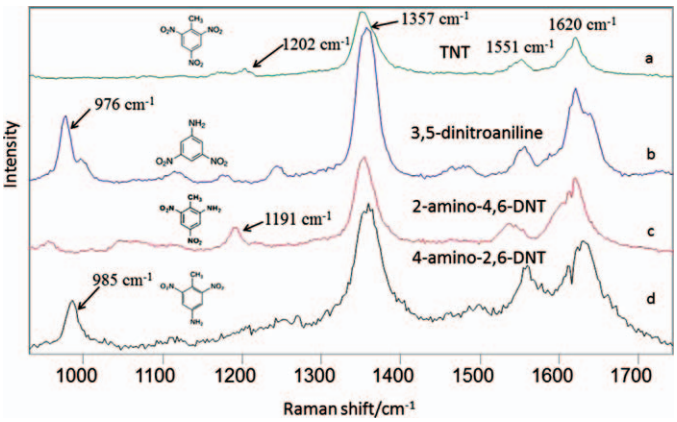

FIG. 9. 229 nm DUVRR spectra of solid TNT and its putative photoproducts on MgF_2 powder: (***a***) TNT, (***b***) 3,5-dinitroaniline, (***c***) 2-amino-4,6-dinitrotoluene, and (***d***) 4-amino-2,6-dinitrotoluene. Spectra are scaled proportional to their Raman cross sections (corrected for self-absorption and instrument function) of the $-NO_2$ symmetric stretching band, at ~1357 cm^{-1}.

DUVRR, the most intense bands derive from $-NO_2$ symmetric and asymmetric stretching vibrations that contain aromatic ring stretching motion.[11,21,22] The DUVRR spectra of TNT and its possible, putative photoproducts in the solid state are similar to those in solution except for small frequency shifts and relative intensity changes.

The solid-state DUVRR cross sections were determined for TNT, 4-amino-2,6-DNT, 2-amino-4,6-DNT, and 3,5-dinitroaniline as shown in Table III. The RR cross sections were determined by using the Na_2SO_4 995 cm^{-1} SO_4^{-2} stretching band as an internal intensity standard.[26]

The cross sections were corrected for the instrument efficiency and for self-absorption following the methods used in Ref. 1. It was assumed that the extinction coefficients for the solution TNT and photoproducts' bands would be the same as for that in the solid state, in order to correct for self-absorption. All of the solid-state DUVRR bands of TNT and the photoproducts have decreased 229 nm cross sections compared to those in solution.

TABLE III. Resonance Raman cross sections at 229 nm of TNT, 2-amino-4,6-DNT, 4-amino-2,6-DNT, and 3,5-dinitroaniline in the solid state.

	Frequencies (cm^{-1})	229 nm resonance Raman cross sections (10^{-26} cm^2/molc·sr)
TNT	1168	0.57
	1202	0.53
	1357	5.5
	1551	1.8
	1620	3.7
2-amino-4,6-DNT	1191	1.8
	1354	8.8
	1540	1.5
	1597	1.6
	1622	5
4-amino-2,6-DNT	985	3.5
	1359	15.1
	1494	2.1
	1565	4.2
	1633	6.6
3,5-dinitroaniline	976	3.5
	1356	16.3
	1477	2.4
	1551	3
	1619	9.13
	1640	5.65

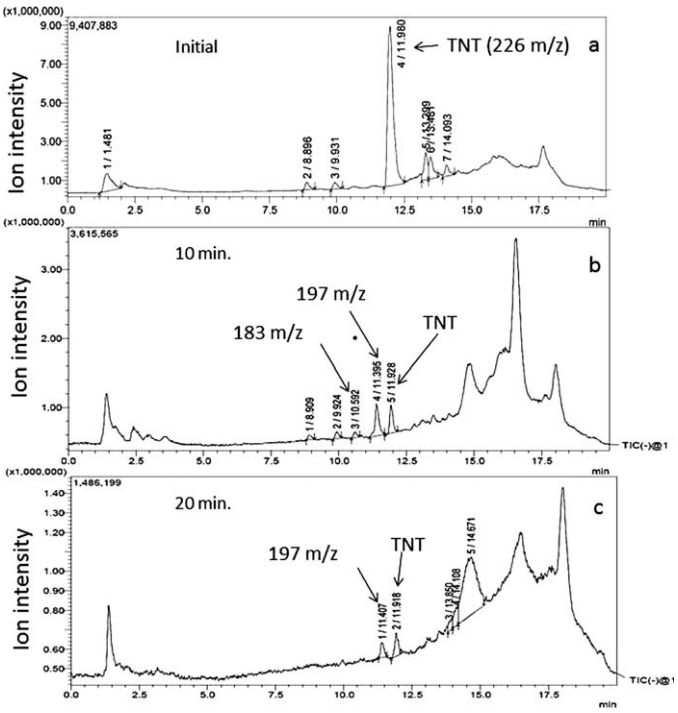

FIG. 10. Time dependence of LC-MS chromatograms of extracted solid TNT irradiated at 229 nm over different time intervals as monitored by their ion current.

To compare the solid-state TNT photochemical products to those in solution, we examined the LC-MS of irradiated solid samples extracted with CH_3CN. Figure 10 shows the mass spectral chromatogram ion currents.

In the absence of irradiation, the chromatogram shows only the TNT peak, while after longer irradiation time, the chromatograms show an attenuated TNT peak and additional peaks at different elution times in a manner similar to the solution state irradiation. Table IV indicates that the photochemistry of solid-state TNT is essentially identical to that of TNT in solution (Table II). The corresponding mass spectra of each chromatogram peak are shown in the Supporting Information section.

CONCLUSION

The TNT signature band at 1210 cm^{-1} in solution and at 1202 cm^{-1} in the solid state derives from a symmetric

TABLE IV. Retention time, m/z, and species present for irradiated solid TNT.

TNT sample	Retention time (min.)	m/z Peak
Initial	12	226
10 min	10.6	183
	11.4	197
	11.9	226
20 min	11.4	197
	11.9	226

aromatic ring breathing motion that is unique to pure TNT. The intensity of this TNT signature band decreases and disappears with 229 nm irradiation, demonstrating that TNT quickly photolyzes with a solution quantum yield of $\varphi \sim 0.015$. In contrast, the intensities of the other peaks in the 229 nm TNT solution and solid-state DUVRR appear to only slowly decrease. This is because the TNT photoproducts have similar bands at very similar frequencies. These bands mainly involve $-NO_2$ stretching vibrations. The dominance of these bands in the TNT Raman spectrum and those of its photoproducts enable highly sensitive DUVRR detection of TNT and its photoproducts even after the complete photolysis of TNT. The similarity of the DUVRR of TNT and its photoproducts enables standoff detection of trace quantities of TNT.

We were able to determine some of the initial TNT photoproducts; 2-amino-4,6-DNT, 3,5-DNA, and 2,5-DNP were confirmed to be initial photoproducts formed. The 2-amino-4,6-DNT and 3,5-DNA are the same photoproducts previously observed in the photochemical degradation of TNT by sunlight.

Trinitrotoluene photolysis at later stages forms an even more complex mixture of photoproducts that dominate the DUVRR spectrum. The TNT degradation Raman spectra show a characteristic class of compounds that consist of $-NO_2$ groups attached to aromatic rings that can be used to sense for TNT in standoff detection.

SUPPLEMENTAL MATERIAL

All Supplemental Material mentioned in the text, including 12 figures and a description of the figures, is available in the online version of the journal, at http://www.s-a-s.org.

1. M. Ghosh, L. Wang, S.A. Asher. "Deep-Ultraviolet Resonance Raman Excitation Profiles of NH_4NO_3, PETN, TNT, HMX, and RDX". Appl. Spectrosc. 2012. 66(9): 1013-1021.
2. D.S. Moore. "Recent Advances in Trace Explosives Detection Instrumentation". Sens. Imaging. 2007. 8: 9-38.
3. D.S. Moore. "Instrumentation for Trace Detection of High Explosives". Rev. Sci. Instrum. 2004. 75(8): 2499-2512.
4. H. Östmark, M. Nordberg, T.E. Carlsson. "Stand-off Detection of Explosives Particles by Multispectral Imaging Raman Spectroscopy". Appl. Opt. 2011. 50(28): 5592-5599.
5. J.C. Carter, S.M. Angel, M. Lawrence-Snyder, J. Scaffidi, R.E. Whipple, J.G. Reynolds. "Standoff Detection of High Explosive Materials at 50 Meters in Ambient Light Conditions Using a Small Raman Instrument". Appl. Spectrosc. 2005. 59(6): 769-775.
6. D.S. Moore, R.J. Scharff. "Portable Raman Explosives Detection". Anal. Bioanal. Chem. 2009. 393: 1571-1578.
7. L.C. Pacheco-Londoño, W. Ortiz-Rivera, O.M. Primera-Pedrozo, S.P. Hernández-Rivera. "Vibrational Spectroscopy Standoff Detection of Explosives". Anal. Bioanal. Chem. 2009. 395(2): 323-335.
8. S. Wallin, A. Pettersson, H. Östmark, A. Hobro. "Laser-Based Standoff Detection of Explosives: A Critical Review". Anal. Bioanal. Chem. 2009. 395: 259-274.
9. I. Johansson, M. Norrefeldt, A. Pettersson, S. Wallin, H. Östmark. "Close-Range and Standoff Detection and Identification of Liquid Explosives by Means of Raman Spectroscopy". In: H. Schubert, none A. Kuznetsov. editors. Detection of Liquid Explosives and Flammable Agents in Connection with Terrorism; NATO Science for Peace and Security Series B: Physics and Biophysics. Dordrecht, NL: Springer, 2008. Pp. 143-153.
10. A. Pettersson, I. Johansson, S. Wallin, M. Nordberg, H. Östmark. "Near Real-Time Standoff Detection of Explosives in a Realistic Outdoor Environment at 55 m Distance". Propellants Explos. Pyrotech. 2009. 34(4): 297-306.
11. D.D. Tuschel, A.V. Mikhonin, B.E. Lemoff, S.A. Asher. "Deep Ultraviolet Resonance Raman Excitation Enables Explosives Detection". Appl. Spectrosc. 2010. 64(4): 425-432.
12. S.A. Asher, C.R. Johnson. "Raman Spectroscopy of a Coal Liquid Shows that Fluorescence Interference is Minimized with Ultraviolet Excitation". Science. 1984. 225(4659): 311-313.
13. L. Wang, D. Tuschel, S.A. Asher. "229 nm UV Photochemical Degradation of Energetic Molecules". Proc. SPIE. 2011. 8018: 80181B-1.
14. M.L. Clark, M.J. Aernecke, K.E. Gregory, D.E. Hardy, R.R. Kunz, A.W. Fountain III. "Sensing Impacts of the Fate of Trace Explosives Signatures under Environmental Conditions". Paper presented at: The 27th Army Science Conference (ASC). Orlando, FL: November 29–December 2, 2010.
15. N.E. Burlinson, L.A. Kaplan, C.A. Adams. "Photochemistry of TNT: Investigation of the 'Pink Water' Problem". Silver Spring, MD: Naval Ordinance Laboratory, Technical Report, 1973.
16. L.A. Kaplan, N.E. Burlinson, M.E. Sitzmann. "Photochemistry of TNT: Investigation of the 'Pink Water' Problem: Part II". Silver Spring, MD: Naval Surface Weapons Center, White Oak Laboratory, 1975.
17. R.R. Kunz, K.E. Gregory, M.J. Aernecke, M.L. Clark, A. Ostrinskaya, A.W. Fountain 3rd. "Fate Dynamics of Environmentally Exposed Explosive Traces". J. Phys. Chem. A. 2012. 116(14): 3611-3624.
18. O. Sandus, N. Slagg. "Mechanism of the Formation of Pink Water". Dover, NJ: U.S. Army Armament Research and Development Command, 1978.
19. S.A. Asher, R.W. Bormett, X.G. Chen, D.H. Lemmon, N. Cho, P. Peterson, M. Arrigoni, L. Spinelli, J. Cannon. "UV Resonance Raman Spectroscopy Using a New cw Laser Source: Convenience and Experimental Simplicity". Appl. Spectrosc. 1993. 47(5): 628-633.
20. S. Bykov, I. Lednev, A. Ianoul, A. Mikhonin, C. Munro, S.A. Asher. "Steady-State and Transient Ultraviolet Resonance Raman Spectrometer for the 193-270 nm Spectral Region". Appl. Spectrosc. 2005. 59(12): 1541-1552.
21. J. Clarkson, W.E. Smith, D.N. Batchelder, D.A. Smith, A.M. Coats. "A Theoretical Study of the Structure and Vibrations of 2,4,6-trinitrotolune". J. Mol. Struct. 2003. 648(3): 203-214.
22. H. Wackerbath, L. Gundrum, C. Salb, K. Christou, W. Viol. "Challenge of False Alarms in Nitroaromatic Explosive Detection—A Detection Device Based on Surface-Enhanced Raman Spectroscopy". Appl. Opt. 2010. 49(23): 4367-4371.
23. W.A. Al-Saidi, S.A. Asher, P. Norman. "Resonance Raman Spectra of TNT and RDX Using Vibronic Theory, Excited-State Gradient, and Complex Polarizability Approximations". J. Phys. Chem. A. 2012. 116: 7862-7872.
24. J.C. Pennington, K.A. Thorn, L.G. Cox, D.K. MacMillan, S. Yost, R.D. Laubscher. "Photochemical Degradation of Composition B and Its Components". Prepared for: Strategic Environmental Research and Development Program. Arlington, VA: U.S. Army Corps of Engineers. Engineers Research and Development Center, 2007.
25. J.M. Dudik, C.R. Johnson, S.A. Asher. "Wavelength Dependence of the Preresonance Raman Cross Sections of CH3CN, SO42-, ClO4- and NO3-". J. Chem. Phys. 1985. 82(4): 1732-1740.
26. L. Wang, D. Tuschel, S.A. Asher. "Templated Photonic Crystal Fabrication of Stoichiometrically Complex Nanoparticles for Resonance Raman Solid Cross Section Determinations". J. Phys. Chem. C. 2011. 115(32): 15767-15771.